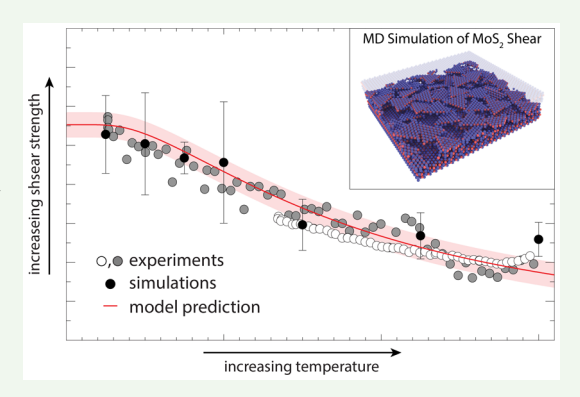
# Atomistic Origins of Temperature-Dependent Shear Strength in 2D Materials

John F. Curry, <sup>†,‡</sup> Adam R. Hinkle, <sup>†,‡</sup> Tomas F. Babuska, <sup>†,§</sup> Mark A. Wilson, <sup>†</sup> Michael T. Dugger, <sup>†</sup> Brandon A. Krick, <sup>§</sup> Nicolas Argibay, <sup>\*,†</sup> and Michael Chandross <sup>\*,†</sup>

ABSTRACT: We present a model that predicts the macroscale temperature-dependent interfacial shear strength of 2D materials like MoS<sub>2</sub> based on atomistic mechanisms and energetic barriers to sliding. Atomistic simulations were used to systematically determine the lamellar size-dependent rotation and translation energy barriers, that were used to accurately predict a broad range of experimental data. This framework provides insight about the origins of characteristic shear strengths of 2D materials.



KEYWORDS: 2D materials, MoS<sub>2</sub>, molybdenum disulfide, nudged elastic band, superlubricity, molecular dynamics, activation energy, temperature

Molybdenum disulfide (MoS<sub>2</sub>) is a lamellar solid with applications in solid lubrication, catalysis, 2D semiconductor-based transistors,<sup>3-5</sup> and photodetectors.<sup>6,7</sup> Many lamellar solids, including MoS<sub>2</sub>, graphite, zirconium phosphate, and hexagonal boron nitride, are useful as tribological materials because weak interactions between lamella provide easy-slip planes that manifest as low friction. Because of this, understanding the interlamellar or interfacial physics is of fundamental and practical value. We establish a fundamental link between the molecular structure of MoS<sub>2</sub> and its temperature-dependent shear strength that is likely applicable to lamellar solids in general. Specifically, we calculated energy barriers for the interlamellar shear of MoS2 and used this information as the basis for a simple model that accurately predicts shear strengths measured by experiments and calculated from molecular dynamics (MD) simulations over a broad range of temperatures.

Regardless of the deposition method, MoS2 naturally tends to order into a nominally defect-free lamellar molecular structure when sheared, having interfacial strength and interlayer separation governed by weak van der Waals forces. Several factors are known to influence the friction of  $MoS_{2}$ including the environment (e.g., oxidation, humidity),<sup>8,9</sup> defects,<sup>10,11</sup> crystallographic texture,<sup>12</sup> and interlamellar spacing.<sup>13,14</sup> As an initial attempt to relate the molecular structure to the tribological response, we focus exclusively on the shear strength of MoS<sub>2</sub> in inert environments, germane to many practical applications and investigations of the superlubricity (i.e., friction coefficients,  $\mu$  < 0.01). Dienwiebel et al. 15 and Verhoeven et al. 16 previously investigated the origins

of the superlubricity of lamellar solids, focusing on the effects of commensurability, or atomic registry, on the friction behavior of graphene. Shear of lamellar solids in general  $^{17-19}$  and  $MoS_2$  in particular  $^{13,14,20,21}$  has been investigated using MD and ab initio simulations, generally focusing on special cases such as commensurate sliding of small MoS<sub>2</sub> lamella<sup>20,21</sup> or the dynamics of MoS<sub>2</sub> lamella in sliding. 13,14 However, it is important to note that commensurate sliding is likely not relevant to shear of lamellar solids because both computational<sup>14,16,22</sup> and experimental<sup>15</sup> investigations have shown that low friction and superlubricity are associated with incommensurate contact.

Early theoretical models developed by Eyring<sup>23</sup> and Prandtl<sup>24</sup> attempted to link fundamental notions of energy barriers and thermally activated processes to macroscopic observations of friction. These models have been further developed or modified by others to account for tribological phenomena. 25-27 Nanoscale friction experiments using atomic force microscopy (AFM) have also been described by theoretical considerations of stick-slip behavior and thermal drift. These considerations were connected to thermally activated jumps over potential energy barriers and used to develop a model of thermolubricity at the atomic scale.<sup>28</sup> In this Letter, we consider MoS<sub>2</sub> as an exemplar 2D material to construct a model that bridges the gap between the molecular

Received: August 21, 2018 Accepted: September 19, 2018 Published: September 19, 2018



<sup>&</sup>lt;sup>†</sup>Material, Physical and Chemical Sciences Center, Sandia National Laboratories, Albuquerque, New Mexico 87123, United States <sup>8</sup>Department of Mechanical Engineering & Mechanics, Lehigh University, Bethlehem, Pennsylvania 18015, United States

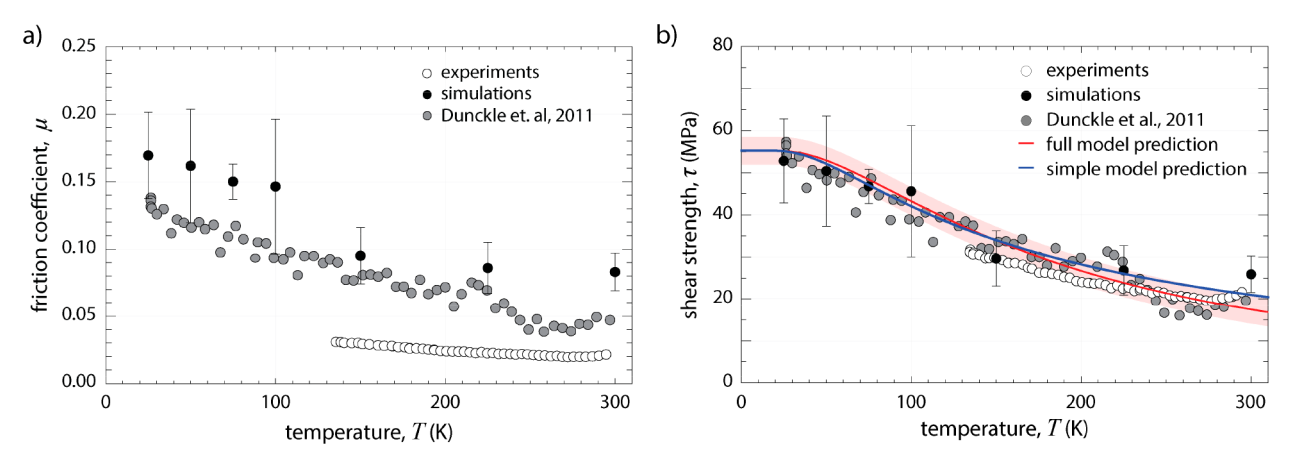


Figure 1. (a) Experimental and MD simulation measured friction coefficients as a function of temperature. (b) Overlay of the experimental and simulation temperature-dependent shear strength data, full model prediction and error bounds based on the uncertainty in  $\tau_0$  from simulations, and simplified model prediction based exclusively on rotation.

origins of interlamellar sliding and macroscopic friction. We systematically calculated the energy barriers to diffusive translation and rotation as a function of the lamellar flake size and commensurability and used these energy barriers as the basis for a predictive model of shear strength as a function of temperature.

Singer et al.<sup>29</sup> showed that pure MoS<sub>2</sub> exhibits a constant or characteristic shear strength of about 25 MPa at room temperature, with a negligible contribution from adhesion. This enabled a simplified definition of the friction coefficient  $\mu$ as the ratio of a characteristic shear strength S and the applied Hertzian pressure,  $\mu = S/P$ . While the work of Singer et al. was only performed at room temperature, multiple reports 30-34 have shown that the friction coefficient of MoS2 changes with temperature. There is notable disagreement in these reports, attributed to the presence of minute amounts of moisture or excessive applied stress.<sup>33,34</sup> Although these earlier reports establish the existence of temperature-dependent friction coefficients, they do not explicitly address the connection between temperature and shear strength, a concept novel to our work. We use data from Dunckle et al.32 as a comprehensive supplemental experimental reference because their work provides the broadest range of temperaturedependent friction coefficient values in a clean, ultrahighvacuum environment.

A comparison of the experimental and simulated friction coefficients and shear strengths of MoS2 over a range of temperatures from 25 to 300 K is presented in Figure 1a,b, with a comparison to the data from Dunckle et al.<sup>32</sup> Shear strengths were extracted from the friction coefficient data of Dunckle et al. using a calculated maximum Hertzian contact pressure of 411 MPa (based on their reported forces) and applying the relationship developed by Singer et al.<sup>29</sup> Our experiments are performed with a variable-temperature friction-testing apparatus<sup>35</sup> using commercially available 300nm-thick initially amorphous<sup>36</sup> magnetron-sputtered pure MoS<sub>2</sub> thin films (Tribologix, Golden, CO) on 440C stainless steel substrates. Counterfaces were 3.2-mm-diameter 440C steel balls at 1 N contact force and 1 mm/s sliding speed. Prior to the temperature ramps, the coatings were run-in to the steady-state friction coefficient ( $\mu \sim 0.05$  at 20 °C), indicating that a thin (5-10 nm) surface film of highly ordered and basally oriented MoS2 was established. The effects of the temperature on the microstructural evolution have not been

assessed. Complementary MD simulations were performed with a reactive force field<sup>37</sup> using a multilayered array of nanoplatelets of MoS<sub>2</sub> sheared between nondefective lamellae at 1 km/s (illustrated in Figure 2a). While this shear velocity is high compared to the experiments, the computational cost of this force field coupled with the large number of simulations necessary to study a wide range of temperatures (at least six different normal loads at eight different temperatures) made it a necessity.

Contact pressures used in the experiments were within the elastic limit, justifying the use of Hertzian contact mechanics.<sup>29</sup> Shear strengths were calculated based on measured friction forces and Hertzian contact area calculations. Singer et al. showed that the measured friction coefficient depends on the applied load, and recent work has also shown that the friction coefficient is temperature-dependent. This motivated our use of  $\tau_0 = \tau$  (T = 0 K) as a material property and characteristic shear strength, and we note that our measurement of  $\tau$  (T =300 K) compares favorably with the value of  $S_0$  by Singer et al. All shear strength data in Figure 1b collapse onto a single curve, exhibiting a smooth dependence on the applied temperature. The remarkable agreement between the MD and experimental data suggests that nanoscale mechanisms are largely responsible for the macroscale friction behavior. These mechanisms are revealed through a study of the energetic barriers to shear via the translation and rotation of flakes.

In order to determine the energy barriers relevant to sliding, we used the nudged elastic band (NEB) method<sup>38,39</sup> to systematically calculate barriers to translation and rotation for a small flake of MoS<sub>2</sub> on top of an infinite lamellar sheet. With an understanding that shear deformation drives initially amorphous MoS<sub>2</sub> to form large, nominally defect-free flakes that are much larger than the sizes accessible to atomistic simulations, it was necessary to determine the dependence of these energy barriers as a function of the flake size and show that, when normalized by the number of atoms in the flake, the barriers converge to values that can be used in the model. In Figure 3, we show the calculated barriers as a function of the flake size for commensurate (Figure 3a) and incommensurate (Figure 3c) sliding. In Figure 3a, we also show the calculated barrier to rotation of the flake, which determines the energetic penalty associated with the change from a commensurate ( $\varphi$  =  $0^{\circ}$ ) to a maximally incommensurate ( $\varphi = 30^{\circ}$ ) state. The commensurability at two different rotation angles is illustrated

ACS Applied Nano Materials Letter

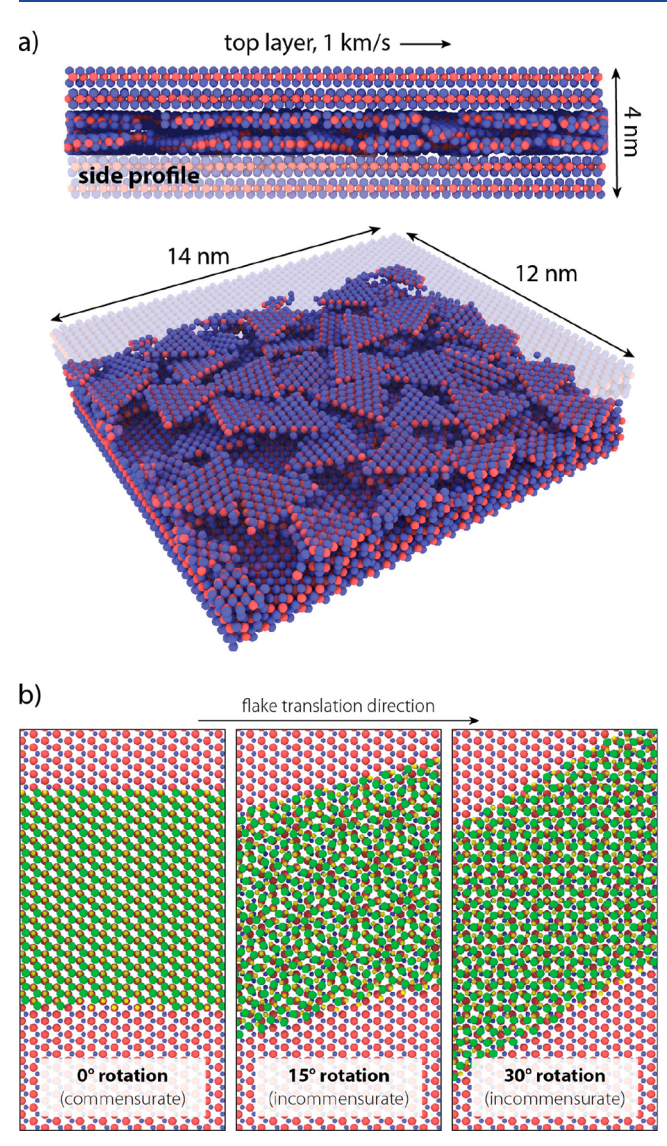


**Figure 2.** (a) 2D cross-sectional and sectioned 3D snapshots of MD simulations. (b) Cropped top-down views of a rectangular flake of  $MoS_2$  on top of a larger sheet to illustrate varying degrees of registry, from commensurate to incommensurate.

in Figure 2b. While even a small rotation angle away from commensurability results in low friction and incommensurate contact during sliding, 14 we used 30° as the prototypical, maximally incommensurate rotation angle. The peak energy barrier values of the converged flake sizes were found to be 36.4, 1.3, and 12.3 meV for commensurate sliding  $(E_c)$ , incommensurate sliding  $(E_i)$ , and pure rotation  $(E_r)$ , respectively, with equivalent temperatures  $(T_n = E_n/k_B)$ provided in Table 1 and used hereafter to reference the barrier values. Our results are in reasonable agreement with previous ab initio computational determinations of commensurate MoS<sub>2</sub> sliding energy barriers, <sup>20,21</sup> validating the potential and NEB approach, but to the best of our knowledge, this is the first calculation of barriers to incommensurate sliding and rotation for MoS<sub>2</sub>. We note that while we and others have found that there exist two barriers to commensurate sliding, 20,21 we did not consider the larger of these barriers (1740 K) in our analysis. As previous work has shown, it is far more energetically favorable to translate along a trajectory that only requires overcoming the smaller barrier (418 K), moving

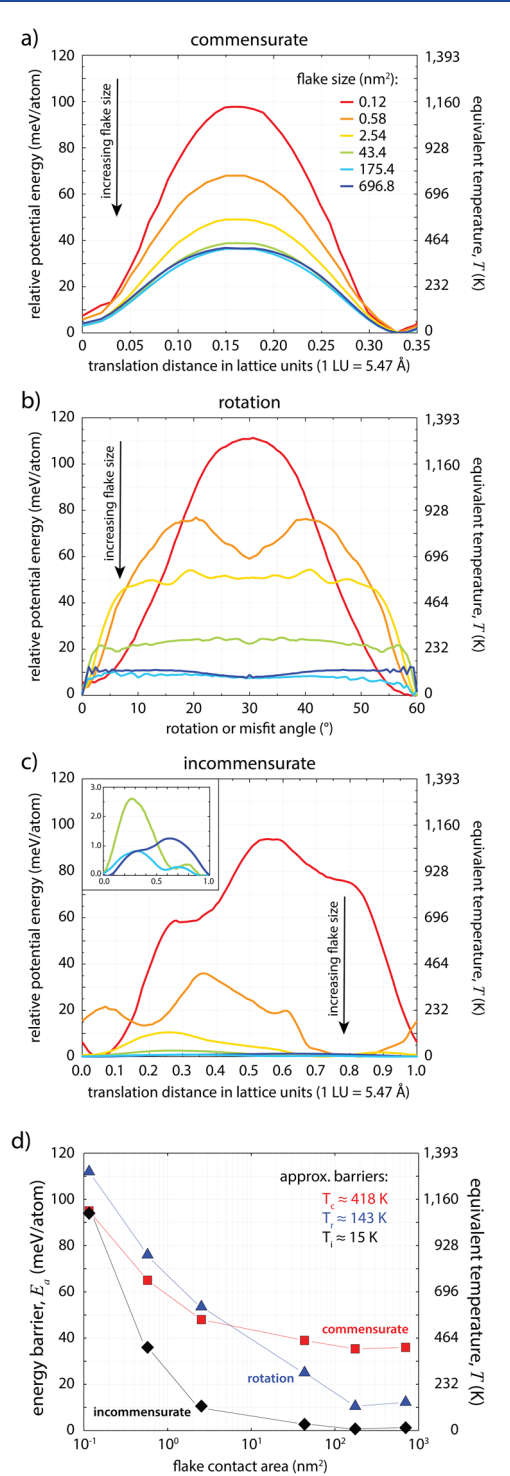


Figure 3. Flake-size-dependent activation energy barriers calculated via the NEB method for (a) translation of flakes while in a commensurate state on an infinite sheet of  $MoS_2$ , (b) rotation of flakes, and (c) translation of flakes while in the incommensurate state (i.e., at  $30^\circ$  rotation). (d) Summary of the flake size dependence of activation energy barriers to translation and rotation, including approximate equivalent temperatures for large flakes.

between sulfur atoms rather than over them.  $^{20,21}$  It is important to note that our assumptions of pure interlamellar sliding and the applicability of the potential energy surfaces require wear rates of the  $MoS_2$  coatings on the order of monolayer removal per sliding pass. Wear rates greater than a

ACS Applied Nano Materials Letter

Table 1. Summary of the Peak Values in Calculated Energy Barriers for a Range of Flake Sizes<sup>a</sup>

		incommensurate translation		pure rotation		commensurate translation	
unit cells <sup>b</sup>	contact area (nm²)	meV/atom	equiv T (K)	meV/atom	equiv T (K)	meV/atom	equiv T (K)
1×1	0.12	94.0	1,090	111	1,290	96.9	1120
2×2	0.58	36.0	418	77.0	893	67.4	782
4×4	2.54	10.5	122	54.2	628	48.6	564
16×16	43.39	2.63	30.5	25.0	290	38.5	446
32×32	175.39	0.841	9.76	10.4	120	35.4	410
64×64	701.11	1.27	14.8	12.3	143	36.1	418

<sup>a</sup>Values are presented in meV/atom and their equivalent temperature of activation. <sup>b</sup>Approximate number of MoS<sub>2</sub> unit cells comprising a flake.

monolayer per pass typically correspond to athermal friction behavior. At sufficiently low wear rates, permitting persistent surfaces, energy barriers can describe the friction behavior. In the temperature range  $100-300~\rm K$ , measured specific wear rates were low, with values in the range  $K\cong 1\times 10^{-6}-1\times 10^{-5}~\rm mm^3/N\cdot m$  (Figure 4); these wear rates imply that, on average, less than 1 monolayer of MoS<sub>2</sub> is removed per sliding pass over the duration of our experiments.

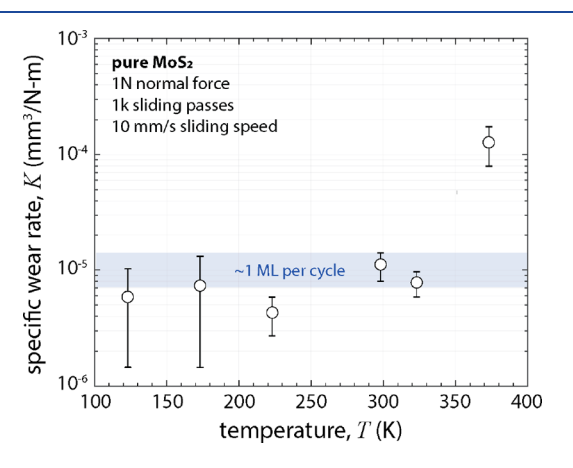


Figure 4. Temperature-dependent specific wear rates for  $MoS_2$  films, showing monolayer/cycle wear rates in the temperature-dependent regime.

The convergence of the energy barriers with the flake sizes that are still in the nanometer range, as seen in Figure 3a-c and summarized in Figure 3d and Table 1, suggests that these values should be generally applicable across a broad range of length scales, from AFM to macroscale experiments. The results in Figure 3d (and summarized in Table 1) show that the incommensurate barrier to sliding is always lower than the commensurate barrier, as expected from the discussion above and prior work. 20,21 The calculated barrier to rotation, however, shows that the overall energy of the commensurate state ( $\varphi = 0^{\circ}$  in Figure 2b) is lower than that of the incommensurate state ( $\varphi = 30^{\circ}$  in Figure 2b). This result shows the importance of understanding the energetic cost to rotation from a commensurate to an incommensurate state. It also demonstrates that while there exist two energetic barriers to incommensurate sliding (i.e., the barrier to rotate to the incommensurate state and the barrier to slide in that state), the combined barrier is still lower than the barrier to commensurate sliding for large flakes. This indicates that incommensurate sliding is always the energetically preferred mechanism for large flakes.

We now show that it is possible to develop a remarkably effective, yet simple model for predicting the temperature-

dependent shear strength  $\tau(T)$  and thus friction coefficient  $\mu(T)$  of MoS<sub>2</sub> based on a combination of these barriers to translation and rotation. We consider two routes for accommodating shear of MoS2 lamellae, namely, commensurate and incommensurate sliding. The Arrhenius equation describes the rate of thermally overcoming an energy barrier  $E_n$ as  $p_n \propto \exp(-E_n/k_BT) = \exp(-T_n/T)$ , where  $k_B$  is the Boltzmann constant and T is temperature. If we consider this expression to represent a probability  $p_n$ , then the failure  $f_n$  to overcome this barrier is  $\hat{f_n} = 1 - p_n$ . We can then write the overall probability for a flake to slide thermally as  $p_{\text{slide}} = p_{\text{r}}p_{\text{i}} +$  $f_{\rm r}p_{\rm c}$  where the two terms in this expression account for the likelihood that a flake must either (1) rotate from commensurate to incommensurate contact and overcome the incommensurate barrier to sliding or (2) fail to rotate and then overcome the commensurate barrier to sliding. The expression above, written in terms of the probability to overcome barriers thermally, describes the probability of lamella sliding diffusively. Friction, however, is associated with the application of a stress to induce sliding, suggesting that we should consider the failure to slide thermally, written as  $f_{\text{slide}} = 1 - p_{\text{slide}} = 1 - p_{\text{slide}}$  $(p_p p_i + f_p p_c)$ . We note that, analogous to the Arrhenius rates, all exponential terms in this expression require a prefactor, and this factor is likely different for each probability. Because we are currently unable to calculate these prefactors, we consider only the exponential form for the dependence on the activation energy and temperature. This approach is clearly not rigorously correct but, nevertheless, uses an appropriate functional form. We then consider the shear strength of the MoS<sub>2</sub> film to be proportional to the failure to slide thermally, converging at T =0 K to the characteristic shear strength  $\tau_0$ . We can then express temperature-dependent shear strength as shown in eq 1.

$$\tau(T) = \tau_0 f_{\text{slide}}$$

$$= \tau_0 \left[ 1 - \exp\left(-\frac{T_{\text{i}} + T_{\text{r}}}{T}\right) - \exp\left(-\frac{T_{\text{c}}}{T}\right) + \exp\left(-\frac{T_{\text{r}} + T_{\text{c}}}{T}\right) \right]$$

$$(1)$$

By using the NEB-calculated barriers for the limiting case of large flakes, shown in Figure 3b,  $\tau_0$  is the only adjustable parameter in eq 1. To arrive at a predictive model with no adjustable parameters, we determined a value for  $\tau_0$  by fitting eq 1 (with various  $T_{\rm n}$  from the NEB calculations) to the temperature-dependent shear strength data from our MD simulations (Figure 1b), arriving at a value of  $\tau_0 = 55.3 \pm 3.1$  MPa. In Figure 1b, we show the results of this model overlaid on the experimental (from our experiments, as well as from Dunckle et al.<sup>32</sup>) and MD simulation data and find remarkable quantitative agreement. We estimated error bounds for this

model based on the uncertainty in the fit for  $\tau_0$  and show this range as the shaded region in Figure 1b. For infinite sheets, the incommensurate barrier is expected to vanish. Additionally, the relatively large barrier to commensurate sliding implies that it should not play a significant role in the frictional response either. We therefore expect that the rotational barrier alone can describe the temperature dependence of the shear strength. To demonstrate this, we remove the contribution of the incommensurate and commensurate translation barriers so that

$$\tau(T) = \tau_0 f_{\text{slide}} \cong \tau_0 (1 - p_{\text{r}}) = \tau_0 \left[ 1 - \exp\left(-\frac{T_{\text{r}}}{T}\right) \right]$$
 (2)

with a single energy barrier,  $T_{\rm r}\cong 143$  K. This simplified model is also overlaid in Figure 1b, again using  $\tau_0=55.3\pm3.1$  MPa. The accuracy of the simplified model across a broad range of temperatures reinforces our claim that commensurate sliding does not play a significant role in the tribological response of MoS<sub>2</sub>, in contrast to prior work. We expect that these effects generalize to other 2D materials (with different energy barriers), in that shear should be dominated by incommensurate sliding, and the necessity to rotate to this state from an initially incommensurate state.

The models presented in eqs 1 and 2 require the use of calculated energy barriers to sliding, and we have chosen to use energy per atom in these expressions. Ignoring finite size effects (a concern at relatively small flake sizes only), as the flake size increases, the total barrier increases linearly with the number of atoms (i.e., contact area). This implies that realistic (i.e., large, experimentally realized) flakes would never diffuse, and our model would lack any predictive power. A similar increase in the barrier height with the size also arises in the related problem of metal island diffusion. 42 In that case, however, it is found that the diffusivity of islands goes as  $\exp(-E_a/kT)N^{\gamma}$ , where  $E_a$  is an unknown, constant energy barrier, N is the number of atoms, and  $\gamma$  is a materialindependent constant.  $^{43,44}$  This expression decouples the Ndependence from the exponential, and the energy per atom is a natural means to arrive at a constant value for  $E_a$ .

The contacts in MoS<sub>2</sub> have already been shown to be elastic, with the implication of sheets sliding over other sheets. This makes the interaction between sheets analogous to an interfacial energy, which is normalized by an area of contact. In the case of lamellar solids like MoS<sub>2</sub>, energy per atom can represent an interfacial energy but with the correct units for use in the Arrhenius-like expressions in eqs 1 and 2. The use of a per-atom barrier is further justified by considering the actual motions of the atoms in both MoS2 and the analogous case of island diffusion. In both cases, the atoms comprising the flake or island do not move as a single, bulk unit but rather by individual edge atoms diffusing first, followed by other atoms in the bulk moving after bonds become stretched.<sup>45</sup> To accommodate this motion in terms of our model, we would need to consider the fraction of atoms with an energy large enough to overcome the barrier, but this would essentially imply a single-atom barrier. In our NEB calculations, the flakes are not held as rigid structures, and visual inspection indicates that atoms do not move rigidly over the sulfur atoms of the substrate layer but rather proceed via their own independent trajectories. Similar atomic-scale movement has also been considered in the motion of polymer chains, 46,47 where the initial translation of individual atoms overcoming a barrier has been interpreted as slip due to dislocations at the end chains.

Dislocation motion has also been discussed in the context of metal island diffusion, where it was found that islands of certain sizes diffuse more quickly than others <sup>48</sup> because of the size-dependent ability to support dislocations. Dislocations are known to exist in  $\text{MoS}_2$  and other lamellar solids, <sup>49</sup> but a study of their contribution to flake motion is beyond the scope of this work. That our model agrees so well with the experimental and simulation values over the complete temperature range implies that a rigorous theoretical justification for our energy barriers likely exists even though at this point it is not yet fully known.

This work establishes a link between the atomistic mechanisms of interlamellar translation of MoS2 and macroscale experimentally measured shear strength. Calculations of the activation energy barriers for the translation and rotation of flakes were used to develop a predictive model based on the temperature-dependent probabilities for commensurate or incommensurate sliding to occur. This model suggests that the energetic barrier to rotation is the dominant factor in the temperature-dependent friction behavior of 2D materials like MoS<sub>2</sub>. The results from experiments and simulations are quantitatively described by this model, using a calculated value of a characteristic shear strength,  $\tau_0$ . The proposed model accurately predicts the friction behavior from a range of sources, including MD simulations and macroscale experiments, and shows excellent agreement across these disparate data sets. This work also presents a basis for the development of more complex models that account for the role of compositing materials (e.g., Sb<sub>2</sub>O<sub>3</sub>, Au, and Ti) and environmental factors (e.g., water vapor).

## AUTHOR INFORMATION

## **Corresponding Authors**

\*E-mail: nargiba@sandia.gov. \*E-mail: mechand@sandia.gov.

### ORCID ®

John F. Curry: 0000-0003-2611-1297 Brandon A. Krick: 0000-0003-3191-5433 Nicolas Argibay: 0000-0002-6473-7568

# **Author Contributions**

<sup>‡</sup>These authors contributed equally to this work.

#### Notes

The authors declare no competing financial interest.

### ACKNOWLEDGMENTS

We thank Greg Sawyer and James Batteas for helpful discussions about temperature-dependent materials' friction behavior. This work was funded by the Laboratory Directed Research and Development program at Sandia National Laboratories, a multimission laboratory managed and operated by National Technology and Engineering Solutions of Sandia, LLC, a wholly owned subsidiary of Honeywell International, Inc., for the U.S. Department of Energy's National Nuclear Security Administration under Contract DE-NA0003525. This material is partially based on work supported by the National Science Foundation under Grant 1752109. Any subjective views or opinions that might be expressed in the paper do not necessarily represent the views of the U.S. Department of Energy or the United States Government.

## REFERENCES

(1) Scharf, T. W.; Prasad, S. V. J. Mater. Sci. 2013, 48, 511-531.

- (2) Kibsgaard, J.; Chen, Z.; Reinecke, B. N.; Jaramillo, T. F. Engineering the Surface Structure of MoS<sub>2</sub> to Preferentially Expose Active Edge Sites for Electrocatalysis. *Nat. Mater.* **2012**, *11*, 963–969.
- (3) Shang, S. L.; Zacherl, C. L.; Fang, H. Z.; Wang, Y.; Du, Y.; Liu, Z. K. Effects of Alloying Element and Temperature on the Stacking Fault Energies of Dilute Ni-Base Superalloys. *J. Phys.: Condens. Matter* **2012**, 24, 505403.
- (4) Lu, C. P.; Li, G.; Mao, J.; Wang, L. M.; Andrei, E. Y. Bandgap, Mid-Gap States, and Gating Effects in MoS<sub>2</sub>. *Nano Lett.* **2014**, *14*, 4628–4633.
- (5) Radisavljevic, B.; Radenovic, A.; Brivio, J.; Giacometti, V.; Kis, A. Single-Layer MoS<sub>2</sub> Transistors. *Nat. Nanotechnol.* **2011**, *6*, 147–150.
- (6) Lopez-Sanchez, O.; Lembke, D.; Kayci, M.; Radenovic, A.; Kis, A. Ultrasensitive Photodetectors Based on Monolayer MoS<sub>2</sub>. *Nat. Nanotechnol.* **2013**, *8*, 497–501.
- (7) Sundaram, R. S.; Engel, M.; Lombardo, A.; Krupke, R.; Ferrari, A. C.; Avouris, P.; Steiner, M. Electroluminescence in Single Layer MoS<sub>2</sub>. *Nano Lett.* **2013**, *13*, 1416–1421.
- (8) Khare, H. S.; Burris, D. L. The Effects of Environmental Water and Oxygen on the Temperature-Dependent Friction of Sputtered Molybdenum Disulfide. *Tribol. Lett.* **2013**, *52*, 485–493.
- (9) Khare, H. S.; Burris, D. L. Surface and Subsurface Contributions of Oxidation and Moisture to Room Temperature Friction of Molybdenum Disulfide. *Tribol. Lett.* **2014**, *53*, 329–336.
- (10) Hoffman, E. E.; Marks, L. D. Soft Interface Fracture Transfer in Nanoscale MoS<sub>2</sub>. *Tribol. Lett.* **2016**, *64*, 1–10.
- (11) Gao, J.; Li, B.; Tan, J.; Chow, P.; Lu, T. M.; Koratkar, N. Aging of Transition Metal Dichalcogenide Monolayers. *ACS Nano* **2016**, *10*, 2628–2635.
- (12) Fleischauer, P. D. Fundamental Aspects of the Electronic Structure, Materials Properties and Lubrication Performance of Sputtered MoS<sub>2</sub> Films. *Thin Solid Films* **1987**, *154*, 309–322.
- (13) Onodera, T.; Morita, Y.; Suzuki, A.; Koyama, M.; Tsuboi, H.; Hatakeyama, N.; Endou, A.; Takaba, H.; Kubo, M.; Dassenoy, F.; Minfray, C.; Joly-Pottuz, L.; Martin, J.-M. M.; Miyamoto, A. A Computational Chemistry Study on Friction of H-MoS<sub>2</sub>. Part I. Mechanism of Single Sheet Lubrication. *J. Phys. Chem. B* **2009**, *113*, 16526–16536.
- (14) Onodera, T.; Morita, Y.; Nagumo, R.; Miura, R.; Suzuki, A.; Tsuboi, H.; Hatakeyama, N.; Endou, A.; Takaba, H.; Dassenoy, F.; Minfray, C.; Joly-Pottuz, L.; Kubo, M.; Martin, J.-M.; Miyamoto, A. A Computational Chemistry Study on Friction of H-MoS<sub>2</sub>. Part II. Friction Anisotropy. *J. Phys. Chem. B* **2010**, *114*, 15832–15838.
- (15) Dienwiebel, M.; Verhoeven, G. S.; Pradeep, N.; Frenken, J. W. M.; Heimberg, J. A.; Zandbergen, H. W. Superlubricity of Graphite. *Phys. Rev. Lett.* **2004**, *92*, 126101–1.
- (16) Verhoeven, G. S.; Dienwiebel, M.; Frenken, J. W. M. Model Calculations of Superlubricity of Graphite. *Phys. Rev. B: Condens. Matter Mater. Phys.* **2004**, *70*, 165418.
- (17) Gao, W.; Tkatchenko, A. Sliding Mechanisms in Multilayered Hexagonal Boron Nitride and Graphene: The Effects of Directionality, Thickness, and Sliding Constraints. *Phys. Rev. Lett.* **2015**, *114*, 096101.
- (18) Restuccia, P.; Ferrario, M.; Sivestrelli, P. L.; Mistura, G.; Righi, M. C. Size-Dependent Commensurability and Its Possible Role in Determining the Frictional Behavior of Adsorbed Systems. *Phys. Chem. Chem. Phys.* **2016**, *18*, 28997–29004.
- (19) Li, S.; Li, Q.; Carpick, R. W.; Gumbsch, P.; Liu, X. Z.; Ding, X.; Sun, J.; Li, J. The Evolving Quality of Frictional Contact with Graphene. *Nature* **2016**, 539, 541–545.
- (20) Liang, T.; Sawyer, W. G.; Perry, S. S.; Sinnott, S. B.; Phillpot, S. R. First-Principles Determination of Static Potential Energy Surfaces for Atomic Friction in MoS<sub>2</sub> and MoO<sub>3</sub>. *Phys. Rev. B: Condens. Matter Mater. Phys.* **2008**, *77*, 104105.
- (21) Levita, G.; Cavaleiro, A.; Molinari, E.; Polcar, T.; Righi, M. C. Sliding Properties of MoS<sub>2</sub> Layers: Load and Interlayer Orientation Effects. *J. Phys. Chem. C* **2014**, *118*, 13809–13816.
- (22) He, G.; Müser, M. H.; Robbins, M. O. Adsorbed Layers and the Origin of Static Friction. *Science* **1999**, 284, 1650–1652.

- (23) Eyring, H. Viscosity, Plasticity, and Diffusion as Examples of Absolute Reaction Rates. J. Chem. Phys. 1936, 4, 283–291.
- (24) Prandtl, L. Ein Gedankenmodell Zur Kinetischen Theorie Der Festen Körper. Z. Angew. Math. Mech. 1928, 8, 85–106.
- (25) Müser, M. H. Velocity Dependence of Kinetic Friction in the Prandtl-Tomlinson Model. *Phys. Rev. B: Condens. Matter Mater. Phys.* **2011**, *84*, 125419.
- (26) Schallamach, A. The Velocity and Temperature Dependence of Rubber Friction. *Proc. Phys. Soc., London, Sect. B* **1953**, *66*, 386.
- (27) Spikes, H.; Tysoe, W. On the Commonality between Theoretical Models for Fluid and Solid Friction, Wear and Tribochemistry. *Tribol. Lett.* **2015**, *59*, 21.
- (28) Krylov, S. Y.; Jinesh, K. B.; Valk, H.; Dienwiebel, M.; Frenken, J. W. M. Thermally Induced Suppression of Friction at the Atomic Scale. *Phys. Rev. E Stat. Nonlinear, Soft Matter Phys.* **2005**, *71*, 065101.
- (29) Singer, I. L.; Bolster, R. N.; Wegand, J.; Fayeulle, S.; Stupp, B. C. Hertzian Stress Contribution to Low Friction Behavior of Thin MoS<sub>2</sub> Coatings. *Appl. Phys. Lett.* **1990**, *57*, 995–997.
- (30) Hamilton, M. A.; Alvarez, L. A.; Mauntler, N. A.; Argibay, N.; Colbert, R. S.; Burris, D. L.; Muratore, C.; Voevodin, A. A.; Perry, S. S.; Sawyer, W. G. A Possible Link Between Macroscopic Wear and Temperature Dependent Friction Behaviors of MoS<sub>2</sub> Coatings. *Tribol. Lett.* **2008**, 32, 91–98.
- (31) Zhao, X.; Phillpot, S. R.; Sawyer, W. G.; Sinnott, S. B.; Perry, S. S. Transition from Thermal to Athermal Friction under Cryogenic Conditions. *Phys. Rev. Lett.* **2009**, *102*, 186102.
- (32) Dunckle, C. G.; Aggleton, M.; Glassman, J.; Taborek, P. Friction of Molybdenum Disulfide-Titanium Films under Cryogenic Vacuum Conditions. *Tribol. Int.* **2011**, *44*, 1819–1826.
- (33) Babuska, T. F.; Pitenis, A. A.; Jones, M. R.; Nation, B. L.; Sawyer, W. G.; Argibay, N. Temperature-Dependent Friction and Wear Behavior of PTFE and MoS<sub>2</sub>. *Tribol. Lett.* **2016**, *63*, 15.
- (34) Curry, J. F.; Babuska, T. F.; Brumbach, M. T.; Argibay, N. Temperature-Dependent Friction and Wear of MoS<sub>2</sub>/Sb<sub>2</sub>O<sub>3</sub>/Au Nanocomposites. *Tribol. Lett.* **2016**, *64*, 18.
- (35) Chandross, M.; Curry, J. F.; Babuska, T. F.; Lu, P.; Furnish, T. A.; Kustas, A. B.; Nation, B. L.; Staats, W. L.; Argibay, N. Shear-Induced Softening of Nanocrystalline Metal Interfaces at Cryogenic Temperatures. *Scr. Mater.* **2018**, *143*, 54–58.
- (36) Moser, J.; Levy, F. J. Crystal Reorientation and Wear Mechanisms in Mos<sub>2</sub> Lubricating Thin-Films Investigated By TEM. *Mater. Res.* **1993**, *8*, 206–213.
- (37) Vasenkov, A.; Newsome, D.; Verners, O.; Russo, M. F.; Zaharieva, R.; van Duin, A. C. T. Reactive Molecular Dynamics Study of Mo-Based Alloys under High-Pressure, High-Temperature Conditions. *J. Appl. Phys.* **2012**, *112*, 13511.
- (38) Henkelman, G.; Uberuaga, B. P.; Jónsson, H. Climbing Image Nudged Elastic Band Method for Finding Saddle Points and Minimum Energy Paths. *J. Chem. Phys.* **2000**, *113*, 9901–9904.
- (39) Henkelman, G.; Jónsson, H. J. Improved Tangent Estimate in the Nudged Elastic Band Method for Finding Minimum Energy Paths and Saddle Points. *J. Chem. Phys.* **2000**, *113*, 9978–9985.
- (40) Burris, D. L.; Perry, S. S.; Sawyer, W. G. Macroscopic Evidence of Thermally Activated Friction with Polytetrafluoroethylene. *Tribol. Lett.* **2007**, *27*, 323–328.
- (41) Blumberg, A.; Keshet, U.; Zaltsman, I.; Hod, O. Interlayer Registry to Determine the Sliding Potential of Layered Metal Dichalcogenides: The Case of 2H-MoS<sub>2</sub>. *J. Phys. Chem. Lett.* **2012**, 3, 1936–1940.
- (42) Shah, S. I.; Nandipati, G.; Kara, A.; Rahman, T. S. Self-Diffusion of Small Ni Clusters on the Ni(111) Surface: A Self-Learning Kinetic Monte Carlo Study. *Phys. Rev. B: Condens. Matter Mater. Phys.* **2013**, *88*, 33–36.
- (43) Karim, A.; Kara, A.; Trushin, O.; Rahman, T. S. The Crossover from Collective Motion to Periphery Diffusion for Two-Dimensional Adatom-Islands on Cu(111). *J. Phys.: Condens. Matter* **2011**, 23, 462201.

- (44) Voter, A. F. Classically Exact Overlayer Dynamics: Diffusion of Rhodium Clusters on Rh(100). *Phys. Rev. B: Condens. Matter Mater. Phys.* **1986**, 34, 6819–6829.
- (45) Uche, O. U.; Perez, D.; Voter, A. F.; Hamilton, J. C. Rapid Diffusion of Magic-Size Islands by Combined Glide and Vacancy Mechanism. *Phys. Rev. Lett.* **2009**, *103*, 046101.
- (46) Dong, H.; Wang, Z.; O'Connor, T. C.; Azoug, A.; Robbins, M. O.; Nguyen, T. D. Micromechanical Models for the Stiffness and Strength of UHMWPE Macrofibrils. *J. Mech. Phys. Solids* **2018**, *116*, 70–98.
- (47) O'Connor, T. C.; Robbins, M. O. Chain Ends and the Ultimate Strength of Polyethylene Fibers. ACS Macro Lett. 2016, 5, 263–267.
- (48) Hamilton, J. C. Magic Size Effects for Heteroepitaxial Islands Diffusion. *Phys. Rev. Lett.* **1996**, 77, 885–888.
- (49) Yazyev, O. V.; Louie, S. G. Topological Defects in Graphene: Dislocations and Grain Boundaries. *Phys. Rev. B: Condens. Matter Mater. Phys.* **2010**, *81*, 195420.